Impacts of the 2019 strong IOD and monsoon events on Indian Ocean sea surface salinity

Ebenezer S. Nyadjro[1]

1. Northern Gulf Institute, Mississippi State University, Stennis Space Center, MS, USA

Remote Sensing in Earth Systems Sciences (RSESS)

**Corresponding Author:*
Ebenezer S. Nyadjro
Northern Gulf Institute
Mississippi State University
1021 Balch Blvd
Stennis Space Center, MS, 39529

esn31@msstate.edu

Abstract

The impact of the 2019 super positive Indian Ocean Dipole (PIOD) event, the strongest in the last four decades, which also co-occurred with an El Niño and a strong summer monsoon, on Indian Ocean sea surface salinity (SSS) is examined using the Soil Moisture Active Passive satellite measurements. Salt budget estimation suggests a predominant, nearly ocean-wide influence by surface freshwater flux and horizontal advective terms. Subsurface ocean influence on the salt budget occurs mainly in the southeastern tropical Indian Ocean (SETIO). The PIOD event suppressed the influence of the El Niño, thereby causing anomalous high precipitation in western India, and leading to an unusual freshening in the southeastern Arabian Sea (AS), which is subsequently advected towards the equatorial Indian Ocean (EIO). In the western Bay of Bengal (BoB), following the waning of monsoon-influenced precipitation in the fall, SSS becomes anomalously salty and traverses towards the AS against the flow of anomalous surface currents. During the peak of the summer monsoon in August-September and the peak of the PIOD event in September-November, SSS in the EIO exhibited tendency for freshening, mainly driven by westward advection of freshwater from the eastern BoB. Conversely, in the SETIO, there was tendency for salinification due to suppression of precipitation, enhanced upwelling of high subsurface salinity, and northward advection of salty water. During December to January of the following year, these salinity tendencies reversed, with salinification in the EIO and freshening in the SETIO.

Key words: Indian Ocean, Sea surface salinity, SMAP, Monsoon, Indian Ocean Dipole.

1. Introduction

Salinity variability in the global ocean is controlled mainly by evaporation, precipitation, river runoff, advection, and entrainment [Delcroix and Henin, 1991; Foltz and McPhaden, 2008; Grodsky et al., 2019; Jury, 2019; Nichols and Subrahmanyam, 2019; Nyadjro et al., 2020]. These controlling factors vary based on ocean state, air-sea interactions, and climate variability [Han and McCreary, 2001; Grunseich et al., 2011; Li et al., 2013; Bingham and Lee, 2017; Subrahmanyam et al., 2018; Qi et al., 2019]. In the Indian Ocean, seasonal reversals of winds during the monsoons impact ocean current magnitudes and directions, which subsequently have contrasting impacts on salinity distributions, especially in the northern basins [Jensen 2001; Nyadjro et al., 2010; Akhil et al., 2014; Trott et al., 2019]. Although located at similar latitudes, the mean sea surface salinity (SSS) in the Bay of Bengal (BoB) and the Arabian Sea (AS) show significant differences (Fig. 1a). While the low SSS in the BoB is caused primarily by precipitation exceeding evaporation, and river runoff, the relatively higher SSS in the AS is primarily due to evaporation exceeding precipitation (Fig.1a).

The India monsoon is a complex air-sea coupled system that impacts rainfall and the livelihood of billions of people. During the southwest (SW) monsoon season in June-September, humid southwesterly winds blow from the ocean towards land and generate about 75% of India's annual rainfall [Murty et al., 1996; Sengupta et al., 2006]. Consequently, river runoff into the BoB is high during this season and tends to affect the variability of SSS in the basin. Indeed, some of the world's largest rivers (e.g. Ganges, Brahmaputra, Godavari, and Irrawaddy) flow into the BoB [Sengupta et al., 2006]. On the contrary, during the northeast (NE) monsoon in November-February, dry and weak northeasterly winds blow from continental Asia towards the ocean. Given the importance of the monsoon to the socio-economic livelihood of the people in the region, studies [e.g. Gadgil et al., 1984; Ashok et al., 2001; Ashok et al., 2004; Behera and Ratnam, 2018; Subrahmanyam et al., 2020] have been dedicated to examining the factors that drive the monsoon and determine its strength and variability. There have been only four strong SW monsoons over the last four decades:1983, 1988, 1994, and 2019 [Roman-Stork et al., 2020]. According to the Indian Institute of Tropical Meteorology, strong monsoons are those whose total rainfall exceeds 10% of the long-term mean.

On interannual scale, the Indian Ocean is impacted by the Indian Ocean Dipole (IOD), a coupled ocean-atmosphere mode that affects both local and global climate variability [Saji et al., 1999; Webster et al., 1999]. The phase and intensity of an IOD event is measured by the Dipole Mode Index (DMI; Fig. 2a), computed as the difference between sea surface temperature anomalies (SSTA) in the western Indian Ocean (50°E-70°E, 10°S-10°N) and the southeastern tropical Indian Ocean (SETIO; 90°E-110°E, 10°S-0°S; Fig. 2b) [Saji et al., 1999]. The IOD typically develops during boreal summer (Fig. 2b) and peaks during September through November (SON; Fig. 2c). During the positive phase of the IOD (PIOD), anomalous winds along the equator are predominantly easterly, and sea surface height anomalies (SSHA) and SSTA are anomalously low (a reverse of the climatologies; Fig. 2d, e) off the coasts of Sumatra and Java in the SETIO [Fig. 2b, e; Saji et al., 1999; Webster et al., 1999]. Consequently, atmospheric convection is suppressed, leading to reduction in rainfall and possible droughts in the countries bordering the SETIO region. The aforementioned scenarios are reversed during the occurrence of the negative phase of the IOD (NIOD) [Saji et al., 1999; Webster et al., 1999]. As the strength of the IOD varies among years, so do the responses of the upper ocean such as exhibited by the SSTA variations over the last three decades in Java and Sumatra (Fig. 2a).

Although the IOD is an intrinsic mode of Indian Ocean variability, it is known to co-occur quite frequently with some El Niño Southern Oscillation (ENSO) events [Saji et al., 1999; Webster et al., 1999; Gnanaseelan et al., 2012]. Consequently, the IOD and ENSO can impact the Indian Ocean both collectively and independently. The 2019 PIOD event is the strongest IOD event thus far during the last four decades and co-occurred with an El Niño [Subrahmanyam et al., 2020; Greaser et al., 2021]. It is reported to have been caused by a strong interhemispheric pressure gradient between a stronger than usual pressure over Australia and a weaker than usual pressure over South China Sea/Philippine Sea which led to a northward flow over the western Maritime Continent that generated a significant air-sea heat flux and thermocline feedback [Du et al., 2020; Lu and Ren, 2020]. According to Wang et al. [2020], the 2019 super PIOD event was associated with the strongest easterly and southerly wind anomalies on record in the SETIO and caused significant latent cooling that overcame the increased radiative warming over the region and led to a unique thermodynamical forcing. The 2019 strong SW monsoon season lasted longer than usual, from June to October [Subrahmanyam et al., 2020], thus overlapping with the development and peak stages of the PIOD event, and potentially affecting each other and SSS variability in the Indian Ocean.

Salinity variability during IOD events is of interest as the anomalies can induce water column instability, which in turn drives upwelling/downwelling. The upwelling of colder subsurface waters into the surface ocean in turn suppresses atmospheric convection, thereby reducing precipitation in the SETIO and beyond [Susanto et al., 2001; Nyadjro and Subrahmanyam, 2014; Horii et al., 2018]. The formation of a barrier layer (i.e. the difference between the mixed layer depth and isothermal layer depth) influences the advection of subsurface saline waters into the surface layers by shielding the usually warm, less saline surface waters from the usually colder, more saline subsurface waters. The barrier layer thus affects the influence that salinity has on air-sea interactions [Masson et al., 2003; de Boyer Montégut et al., 2004].

The unusual co-occurrence of the strongest IOD event since 1979, the strongest SW monsoon event since 1994, and an El Niño event, motivates this study to examine the response of the Indian Ocean SSS to these events that occurred during 2019. The increased volume of data from satellite salinity measurements such as the Soil Moisture and Ocean Salinity (SMOS) and the Soil Moisture Active Passive (SMAP) missions have enabled the examination and understanding of SSS variability during such interesting climatic events.

2. Data and Methods

2.1 Data

Monthly 0.25°×0.25° gridded Level-3 SSS data from April 2015 to present were obtained from the SMAP v5.0 product produced by the National Aeronautics and Space Administration (NASA) Jet Propulsion Laboratory (JPL; https://smap.jpl.nasa.gov/data/) and distributed by the NASA Physical Oceanography Distributed Active Archive Center (PO.DAAC). The SMAP satellite measures brightness temperature using the L-band (1.4 GHz) at a spatial resolution of 40 km every 3 days, from which SSS is then derived. In a recent assessment of SMAP, Menezes [2020] showed it to be statistically reliable in the Indian Ocean due to its improved spatial resolution, and enhanced correction of radio frequency interferences and land contamination, thereby enhancing its reliability for coastal area studies.

Daily SST data on a 0.25°×0.25° grid were obtained from the National Oceanic and Atmospheric Administration (NOAA) National Centers for Environmental Information (NCEI) Optimum Interpolation Sea Surface Temperature (OISST) v2.1 product. The OISST product is produced by combining observations from different platforms such as from ship measurements, buoys, Argo floats and satellites (e.g. from the Advanced Very High-Resolution Radiometer -AVHRR- infrared satellite) [Reynolds et al., 2007]. The OISST data spans from 1982 to present.

We obtained surface wind data from the v2.0, 6-hourly ocean gap-free 0.25°×0.25° gridded Remote Sensing Systems' (RSS) Cross-Calibrated Multi-Platform (CCMP) product [Mears et al., 2019]. This product, available from 1988 to present, is produced by combining cross-calibrated satellite microwave winds and instrument observations using a Variational Analysis Method (VAM). Daily precipitation data on a 1°×1° grid and available from 1996 to present, are from the University Corporation for Atmospheric Research (UCAR) Global Precipitation Climatology Product (GPCP) v2.2 product archived at NOAA NCEI [Huffman et al., 2012]. The GPCP data are produced from a combination of rain gauge and satellite data. We used monthly 0.25°×0.25° gridded evaporation data obtained from the European Centre for Medium-Range Weather Forecasts ERA5 data set. This data set is available for 1979 to present.

Daily mean sea surface height anomaly (SSHA) data on a 0.25°×0.25° grid were obtained from Archiving, Validation, and Interpretation of Satellite data in Oceanography (AVISO) [Ducet et al., 2000]. This product is produced by merging SSH from altimetry satellites such as the European Remote Sensing Satellite (ERS-1/2), Ocean Topography Experiment (TOPEX)/Poseidon, Jason-1, Jason-2, Jason-3, Sentinel-3A, Saral/AltiKa, and Cryosat-2. The product is distributed by Copernicus Marine and Environment Monitoring Service (CMEMS) (http://www.marine.copernicus.eu). Surface velocity currents for this study are from the Ocean Surface Current Analyses Real-Time (OSCAR) data set [Bonjean and Lagerloef, 2002]. OSCAR currents are produced by combining satellite-derived ocean surface heights, surface winds, and SST using a diagnostic model of ocean currents based on frictional and geostrophic dynamics. OSCAR data are available at a spatial resolution of 1°×1° and represent mean currents in the upper 30 m of the ocean.

Subsurface 0.5°×0.5° gridded temperature and salinity data obtained from the Coriolis Ocean Database Reanalysis (CORA v5.2; Cabanes et al. 2013) were used in this study. The CORA product is produced by objective analysis of data from several sources such as Argo floats, moorings, sea mammal, Conductivity-Temperature-Depth (CTD), eXpendable CTDs (XCTD), and expandable bathythermographs (XBTs).

Monthly mean fields are computed from daily mean fields. Interannual anomalies are computed by subtracting the monthly climatologies from the monthly time series and then smoothing with a 3 month running mean twice to remove intraseasonal variability.

2.2 Methods

Mixed layer depth (MLD) was computed from CORA using a variable density threshold equivalent to 0.2 °C [de Boyer Montégut et al., 2004]:

$$\Delta\sigma_\theta = \sigma_\theta(T_{10} - 0.2, S_{10}, P_0) - \sigma_\theta(T_{10}, S_{10}, P_0) \qquad (1)$$

where $\Delta\sigma_\theta$ is the change in potential density between the reference depth (10 dbar) and the base of the mixed layer. T_{10} and S_{10} are respectively temperature and salinity at 10 dbar, and P_0 is sea surface pressure. The isothermal layer depth (ILD) is computed as the depth at which the subsurface temperature decreases by 0.2 °C relative to the temperature at the reference depth of 10 dbar. The barrier layer thickness, BLT = ILD-MLD. Thus, from the above definitions, there is no barrier layer when the temperature controls the MLD (i.e. MLD ≈ ILD). Conversely, a barrier layer will occur when the salinity stratification is different from temperature stratification (de Boyer Montégut et al., 2004).

We computed the SMAP salt budget following similar approach in Zhang et al. [2013], Akhil et al. [2016], and Kido and Tozuka [2017]:

$$\frac{\partial S\prime}{\partial t} = \bar{S}\frac{(E-P)\prime}{h} - \bar{u}\frac{\partial S'}{\partial x} - u'\frac{\partial \overline{S}}{\partial x} - \bar{v}\frac{\partial S'}{\partial y} - v'\frac{\partial \overline{S}}{\partial y} - w'\frac{\partial \overline{S}}{\partial z} + R \qquad (2)$$

where overbar terms represent climatological mean seasonal cycle and primed terms represent interannual variability. S is SMAP salinity, h is MLD, E is evaporation, P is precipitation, u is zonal current velocity, v is meridional current velocity, and w is vertical current velocity. We computed w by combining the Ekman upwelling (w_e) and vertical motion of the MLD ($\frac{\partial h}{\partial t}$), $w = w_e + \frac{\partial h}{\partial t}$, where $w_e = curl\left(\tau/_f\right)\rho^{-1}$, τ is wind stress, f is Coriolis parameter and ρ is the surface density computed from the CORA data. The residual R from the computation represents physical processes such as lateral and vertical mixing processes that cannot be estimated directly from the dataset. We estimated the vertical salinity gradient from the CORA data as the difference between SSS and salinity 10 m below the MLD. The terms in equation (2) from left to right are the anomalous salinity tendency, anomalous sea surface freshwater flux of the mean salinity, zonal advection of anomalous salinity by the climatological zonal current, zonal advection of climatological salinity by the anomalous zonal current, meridional advection of anomalous salinity by the climatological meridional current, meridional advection of climatological salinity by the anomalous meridional current, anomalous interaction of the mixed layer with the layer below, and residuals. The net zonal advection anomaly $UADV = -(\bar{u}\frac{\partial S'}{\partial x} + u'\frac{\partial \overline{S}}{\partial x})$, while the net meridional advection anomaly $VADV = -(\bar{v}\frac{\partial S'}{\partial y} + v'\frac{\partial \overline{S}}{\partial y})$.

3. Results and Discussion

3.1. Mean SMAP SSS

The mean SSS in the Indian Ocean as depicted by different datasets in previous studies [e.g. Masson et al., 2003; Rao and Sivakumar, 2003; Akhil et al., 2014; Nyadjro et al., 2014; D'Addezio et al., 2015] is well reproduced by SMAP (Fig. 1a). Mean SSS is high in the AS due to evaporation exceeding precipitation. On the other hand, mean SSS is low in the BoB due to monsoon-influenced precipitation and river-runoff exceeding evaporation [Fig. 1a]. Relatively low SSS is also seen along Java-Sumatra and is influenced by fresh waters from the BoB and from the Pacific Ocean via the Indonesian Throughflow [ITF; Susanto et al., 2001; Sengupta et al., 2006].

In the Indian Ocean, dominant SSS variability occurs in the northern basins, equatorial region, and the SETIO (Fig. 1a, b). SSS seasonal variability is strongest in the northern Indian Ocean (NIO), especially in the BoB (Fig. 1b) due to seasonal reversing monsoon winds, seasonal reversing currents and significant changes in precipitation and river runoff over the course of the seasons [Jensen, 2001; Chaitanya et al., 2014]. Also, there is strong SSS seasonal variability along the coast of Sri Lanka as it is the pathway for exchange of salty and freshwater between the AS and BoB. In the AS, SSS seasonal variability occurs mainly in the eastern rim and southeastern AS. The central equatorial Indian Ocean and SETIO show relatively marginal SSS seasonal variability (Fig. 1b). On interannual scale, the NIO is still the most variable area, albeit less energetic than the seasonal variability, while the southern BoB, eastern AS, Sri Lanka and SETIO regions show relatively weaker interannual SSS variability (Fig. 1c). The interannual variability is controlled primarily by the IOD, but further strengthened when the IOD co-occurs with ENSO [Thompson et al., 2006; Grunseich et al., 2011; Nyadjro et al., 2014].

3.2. SSS in the Northern Indian Ocean

In Fig. 3, we assess the SMAP SSS seasonal cycle in the NIO to provide context for the examination of variability during the 2019 strong monsoon and PIOD events. Time series plots of SSS seasonal anomalies (Fig. 3a), box-averaged along the pathways of water exchange in the NIO (Fig. 3b), highlight the SSS variations that occur across the monsoon seasons. At the peak of the SW monsoon season in August, increased precipitation, and river runoff caused freshening of the surface ocean in the northern BoB (Fig. 3b). The West India Coastal Current (WICC) is southward in the eastern AS, the southwest monsoon current (SMC) is eastward south of Sri Lanka, while the East India Coastal Current (EICC) is northward in southwestern BoB (Fig. 3b; see also McCreary et al., 1996; Schott and McCreary, 2001), suggesting, and supporting, the advection of high salinity waters from the AS into the BoB to balance the lowered SSS in the BoB. Consequently, SSS along southern India and Sri Lanka is saltier than the annual mean as high salinity water is transported from the AS into the BoB (Fig. 3a). During the intermonsoon break in October, the currents, especially those south of Sri Lanka, weaken (Fig. 3d).

The aforementioned currents begin to reverse prior to the start of the NE monsoon [Fig. 3e; Schott and McCreary, 2001]. At this time, the low salinity waters in the northern BoB begin to spread out of the bay towards Sri Lanka. At the beginning of the NE monsoon season in November, the EICC is southward along the southwestern BoB coast, the northeast monsoon current (NMC) is westward south of Sri Lanka while the WICC is northward in southeastern AS (Fig. 3e), consistent with previous reports [e.g. Murty et al., 1992; McCreary et al., 1996; Schott and McCreary, 2001]. This current structure persists into the peak of the NE monsoon in January and flushes out freshwater from the BoB into the AS via southern India and Sri Lanka (Fig. 3g). The spreading of fresh surface waters in the southwestern BoB intensifies during November to December as the EICC strengthens (Fig. 3a, e-f). The freshwater is pushed into the AS during January to March by the westward NMC and northward WICC (Fig. 3g-i). During this time, the northern BoB becomes relatively saltier (Fig. 3g-i) as the influence of the summer monsoon-driven precipitation and river runoff had waned (Fig. 3). Another pathway for the export of the excess BoB freshwater from the SW monsoon, as suggested by Han and McCreary [2001] and Rao and Sivakumar [2003], is the eastern BoB, where coastal currents and waves advect the water towards the equatorial region and Indonesia (Fig. 3).

SSS and surface currents in the NIO underwent significant changes during the 2019 strong monsoon and PIOD events (Fig. 4). Relative to August climatology, there is freshening of ~1 PSU along the southeastern AS coast, which is subsequently advected by the anomalous WICC towards Sri Lanka and the equatorial Indian Ocean (Fig. 4b). Previous studies [e.g. Thompson et al., 2006; Nyadjro et al., 2014] have suggested the eastern BoB to be the source of freshwater in the equatorial Indian Ocean during the occurrence of PIOD events (Fig. 4d-f). Our result suggests that the southeastern AS is an additional source of low salinity waters to the equatorial Indian Ocean during strong PIOD events (Fig. 4d-f). The surface freshening in the southeastern AS was possibly caused by the anomalous, increased precipitation in the region during August 2019 (Fig. 5b). Such high precipitation during August is quite unusual as the prior years show relatively lower precipitation during July-August (Fig. 5a).

A recent study by Ratna et al. [2021] suggests that the co-occurrence of a strong PIOD and a relatively weaker ENSO (as occurred in 2019) leads to wetter India summer monsoons. The study showed that India summer monsoon rainfall was 16% greater during 2019, with regards to the 1981-2010 climatology. Typically, India summer monsoon rainfall is suppressed in an El Niño only year [Behera and Ratnam, 2018] or when a weak/moderate PIOD co-occurs with a strong El Niño year [as occurred in 2015; Zhang et al., 2018]. However, when a strong PIOD and a relatively weaker El Niño co-occur, the PIOD event influences an increase in rainfall over India while also suppressing the El Niño's negative impact on the Indian Ocean monsoon [Ashok et al., 2001; Ashok et al., 2004; Anil et al., 2016; Behera and Ratnam, 2018]. Ashok et al [2004] showed that during such occurrences, an anomalous divergence center forms over the eastern tropical Indian Ocean from where an anomalous divergent flow crosses the equator, weakens El Niño-induced divergence over the western Pacific, and strengthens convergence over the Indian Ocean monsoon area. Subsequently, there is an increase in rainfall especially over western India. The anomalous, increased rainfall over western India persists into October 2019 (Fig. 5c, d) and influences the occurrence of the anomalous low surface salinity waters seen in the southeastern AS during this period (Fig. 4c, d). This is at variance with the 2015 PIOD event where the strong El Niño suppressed precipitation in the western Indian Ocean during the boreal summer (Fig. 5a) and caused positive SSS anomalies in the southeastern AS (Fig. 4a).

Besides the increased precipitation in the western Indian Ocean during 2019, there were anomalously warm thermocline waters along the pathways of water exchange in the NIO during the peak of the PIOD, differing from what occurred during similar period in 2018 (Fig. 6d-f). In addition, barrier layers formed along these pathways (Fig. 6) which strengthened stratification, and inhibited mixing of the anomalous fresh surface waters with the saltier subsurface ocean in the southeastern AS thereby prolonging the presence of the freshwater pool in the southeastern AS into November 2019 (Fig. 4e). The formation of a barrier layer in this region helps sustain high SST (>28°C) which subsequently promotes deep atmospheric convection and heavy precipitation [Gadgil et al., 1984; Nyadjro et al., 2012]. In the southwestern BoB, the barrier layer restrained mixing of the anomalous salty SSS with the fresher subsurface ocean (Fig. 4c) thereby enabling the salinification of the southwestern BoB surface ocean to linger on longer during the PIOD event (Fig. 4).

The extent of the anomalous freshening in the southeastern AS (Fig. 4) is not properly resolved in other datasets examined (e.g. Argo and CORA, Figure not shown), thus showing the superiority of SMAP data in this regard. Indeed, Chaitanya et al. [2014] posited similar limitations when they showed the inability of in-situ observations in capturing the amplitude and narrow offshore structure of a freshening event in the NIO. Such limitation was primarily attributed to excessive spatial smoothing resulting from paucity of in-situ measurements.

As the PIOD peaks during October-December and the monsoon-influenced rainfall wanes in the BoB (Fig. 5d-f), the sea surface becomes anomalously saltier in the northern BoB, and traverses along the western BoB coast, via southern Sri Lanka into the AS (Fig. 4d-g). This movement of anomalous high salinity water out of the BoB is against the flow of the anomalous northward-flowing EICC (Fig. 4d-g). Such export of high salinity surface water during October-January is at variance with what happens in the seasonal cycle when freshwater is exported by the southward-flowing EICC towards the AS (Fig. 3d-g; see also Jensen 2001; D'Addezio et al. 2015; Trott et al., 2019). The EICC often flows southward during the NE monsoon and northward during the SW monsoon [McCreary et al., 1996; Shankar et al. 1996]. It is however strongly impacted by remote forcing through Kelvin waves, which causes it to occasionally oppose local winds and flow in unexpected directions [McCreary et al., 1996; Rao et al., 2010; Dandapat et al., 2018; Fournier et al., 2017]. In addition, westward-travelling Rossby waves, forced by variable winds in the interior of the BoB, impact the EICC [McCreary et al., 1996; Shankar et al., 1996; Greaser et al., 2021]. A study by Dandapat et al. [2018] suggests that the EICC is most unstable, disorganized, and weak during PIOD events. Further, a modelling study by Akhil et al. [2016] and satellite study by Fournier et al. [2017] suggest that PIOD events tend to generate large-scale sea level anomalies and anticyclonic flows near the coastal areas of the western BoB Thus these mesoscale eddies, rather than the EICC, may have driven the export of anomalous high salinity waters out of the BoB during the peak of the 2019 PIOD event.

3.3. SSS in the Equatorial Indian Ocean

The climatological equatorial westerly winds (Fig. 2d, e) reverse to be easterly winds during the PIOD event (Fig. 2b, c) and generate anomalous westward currents in the surface equatorial Indian Ocean (Fig. 4). SSS anomalies were weak in the equatorial region prior to the peak of the PIOD event (Fig. 4b, c). Surface equatorial waters freshened during the peak of the 2019 PIOD event, between October 2019 and January 2020 (Fig. 4d-g), with peak negative SSS anomalies during December (Fig. 4f). The freshening was caused by the anomalous, increased precipitation in the equatorial region during this period (Fig. 5d-g). In addition, anomalous, fresh surface waters were sourced from the southeastern AS (as earlier mentioned) and the eastern BoB, with the later advected westward towards the western equatorial Indian Ocean by the strengthened, anomalous equatorial surface currents (Fig. 4), consistent with results from Thompson et al. [2006], Zhang et al. [2013], and Nyadjro and McPhaden [2014].

3.4. SSS in the SETIO

SSS variability in the SETIO is strongly correlated with the IOD, with the DMI leading the SSS variability by a month (Fig. 4a). Typically, positive (negative) SSS anomalies occur in Java and

Sumatra during PIOD (NIOD) events (Fig. 4a). Enhanced upwelling and reduced precipitation (Fig. 5) during the 2019 PIOD event led to positive SSS anomalies in the SETIO (Fig. 4). Salinification of the SETIO surface ocean was first noticeable during August 2019, especially in the northwestern Java and southwestern Sumatra coasts. By October 2019, during the peak of the PIOD event, the salinification has increased, covering much of the Java-Sumatra coast, and also spread further offshore by the anomalous currents (Fig. 4). The SETIO salinification reached its peak during November 2019, at which time it exceeded 1.5 PSU. Noteworthy is that the SETIO salinification continued beyond the PIOD event into 2020, as the driving mechanisms have not entirely disappeared and also consistent with the cycling of wave energy during IOD events as suggested by Gnanaseelan et al. [2012], McPhaden and Nagura [2014], and Nyadjro and McPhaden [2014].

There are regional differences in SSS distribution in the SETIO with SSS variability in Java and Sumatra being out of phase in certain years (Fig. 4a). For example, during the fall of 2015 and 2018, SSS anomalies were positive in Java but negative in Sumatra (Fig. 4a). During the peak of the 2019 PIOD event, salinification was stronger along the Sumatra coast than along the Java coast. For example, at the peak of the salinification in November 2019, SSSA was 0.8 PSU at Sumatra and 0.65 PSU at Java (Fig. 4a). Possible reasons for the SETIO regional differences include the anomalous southeasterly winds being stronger and more upwelling-favorable (i.e., stronger alongshore winds) along Sumatra than along Java (Fig. 2b, c), as well as Kelvin wave activities that are dominant along the Sumatra coast [Murtugudde et al., 2000]. Subsequently, there was a stronger upwelling (i.e. see the displacement of isotherms; Fig. 7) of salty waters in Sumatra than Java (Fig. 4). There is also an additional influence from the ITF which brings warm, freshwater from the Pacific Ocean that potentially lowers the salinity in Java but has little or no influence in Sumatra [Susanto et al., 2001; Du et al. 2005; Sengupta et al., 2006; Hu and Sprintall, 2016].

3.5. Subsurface influence in the SETIO

The subsurface ocean plays an important role in SSS variability. There was stronger upwelling of anomalously high salinity (>0.5 PSU) and colder waters (<-3°C) from the subsurface during the 2019 PIOD event than during comparable periods in 2018 (Fig. 7). This was caused by stronger displacements of the isotherms during 2019 than during 2018 (Fig. 7d-f). While the summer deepening of the MLD is comparable in both years, the ILD is weaker during 2019 than 2018. In addition, unlike in 2018, both the MLD and ILD are similar during the PIOD event in 2019. Subsequently, there was no barrier layer formation during the PIOD event, hence enabling the stronger vertical advection of saltier, colder waters into the SETIO surface ocean. In turn, the salinification of the surface ocean destabilizes the water stratification, inducing vertical mixing over the water column and enhancing further SST cooling in the SETIO [Kido and Tozuka, 2017; Horii et al., 2020]. Regionally, the mixed layer salinification and cooling are stronger in Sumatra than in Java (Fig. 7) due to reasons previously ascribed.

3.6. SSS budget

The processes responsible for the salinity variability during the 2019 strong PIOD and summer monsoon events are examined in a salt budget estimation (Fig. 8). Salinity tendency was controlled predominantly by the surface freshwater flux and horizonal advective (mainly the zonal advection of climatological salinity by the anomalous zonal current, i.e. term 4 in equation

(2); Figure not shown) terms. The influence of the subsurface term (i.e. term 7 in equation (2)) on the SSS budget is minimal in most areas of the Indian Ocean and therefore not shown. During the SW monsoon season, the freshwater flux term showed tendency for freshening in the NIO (Fig. 8e, f) and contributed immensely to the surface freshening observed in the southeastern AS (Fig. 8b-e). In the BoB however, the freshening tendency by the freshwater flux term was overwhelmed by salinification tendency by the horizontal advection terms (Fig. 8i, j, m, n), hence the mostly positive SSS anomalies observed in the northern BoB (Fig. 4). In addition, previous studies [e.g. Akhil et al., 2014; D'Addezio et al. 2015; Pant et al., 2015] have suggested that vertical advection of salty subsurface waters tend to balance the impact of surface freshwater flux and river runoff during the SW monsoon in the northern BoB, such that it suppresses the lowering of the salinity tendency.

The tendency for surface freshening in the equatorial Indian Ocean during the PIOD event was largely controlled by surface freshwater flux term where precipitation exceeded evaporation (Fig. 8e-h), and the zonal advection term which brought freshwater from the eastern rim of the BoB towards the central and western equatorial Indian Ocean (Fig. 8i-l). The usual semi-annual eastward-flowing Wyrtki jets that occur during the intermonsoon in October-November is not present during the peak of the PIOD event [Masson et al., 2003]. Instead, a westward flow develops and advects freshwater along the equatorial region. In the SETIO, there was tendency for salinification during the boreal summer which strengthened during the peak of the PIOD event in the boreal fall. This is driven mostly by the anomalous sea surface freshwater flux of the mean salinity term in which evaporation exceeded precipitation (Fig. 8e-h) with maximum influence occurring during October-November (Fig. 8g). The salinification is further augmented by upwelling of anomalous high subsurface salinity (Fig. 7), and northward advection of high salinity waters along the Java-Sumatra coast (Fig. 8m-p). The upwelling of anomalous cold water (Fig. 7d-f) potentially suppresses atmospheric convection and precipitation which further sustains the salty surface ocean in the SETIO [Susanto et al., 2001; Kido and Tozuka, 2017; Horii et al., 2020; Wang et al., 2020].

4. Summary and Conclusions

The co-occurrence of the strongest PIOD event since 1979, the strongest SW monsoon event since 1994, and an El Niño event provided a unique opportunity to use SMAP satellite-derived data to examine the response of the Indian Ocean SSS to these events that occurred during 2019. SMAP is able to reproduce the observed, known features of SSS variability in the Indian Ocean, and thus gives confidence in the results obtained in this study. Overall, the anomalous sea surface freshwater flux of the mean salinity and zonal advection of climatological salinity by the anomalous zonal current terms of the salt budget equation were the dominant factors controlling SSS variability in the Indian Ocean during 2019. There were notable changes in SSS in the NIO as a result of the co-occurrence of a strong monsoon with strong PIOD and El Niño events. Most importantly, an unusual anomalously fresh SSS occupied the southeastern AS during the summer monsoon and PIOD events, driven by PIOD-influenced anomalous precipitation in the western Indian Ocean. Meanwhile, in the BoB, the usual impact of precipitation was suppressed, which, together with advective processes, caused positive SSS anomalies that were subsequently exported out of the bay.

In the equatorial Indian Ocean, anomalous precipitation (Fig. 5), and westward advection of less saline waters from the eastern Indian Ocean (Fig. 4) led to freshening. In the SETIO however, strong upwelling-favorable southeasterly winds which is influenced by the co-occurrence of PIOD and ENSO, occurred along the Java-Sumatra coast. These drove water away from the coast, enabling an upwelling of colder, saltier subsurface waters into the surface ocean. This process, together with anomalous net evaporation, and northward advection of high salinity water, led to a significant salinification in the SETIO during the 2019 strong PIOD event. In summary, the co-occurrence of multiple ocean-climate events leads to quite unusual variability of SSS in the Indian Ocean. Additional studies will be needed to completely understand how these interactions and variabilities further feed back to impact these events and oceanic and atmospheric parameters in the Indian Ocean and beyond.

Acknowledgments

The author duly acknowledge the various data sources for the freely available data. Thanks to Bennet Atsu Foli for helping proofread the manuscript. Thanks to the anonymous reviewers whose comments helped improve the manuscript.

Conflicts of interest/ Competing interests: Authors declare no financial and competing interests.

Code availability: None.

Availability of data and material:

SMAP SSS data are available at https://smap.jpl.nasa.gov/data/. OISST data are available at https://www.ncei.noaa.gov/data/sea-surface-temperature-optimum-interpolation/v2.1/access/avhrr/. GPCP precipitation is downloaded from https://www.ncei.noaa.gov/data/global-precipitation-climatology-project-gpcp-daily/access/. SSH data are available at http://www.marine.copernicus.eu. ERA5 data is downloaded from https://cds.climate.copernicus.eu/cdsapp#!/dataset/reanalysis-era5-single-levels-monthly-means?tab=overview.

References

Akhil VP, Durand F, Lengaigne M, Vialard J, Keerthi MG, Gopalakrishna VV, Deltel C, Papa F, de Boyer Montegut C (2014) A modeling study of the processes of surface salinity seasonal cycle in the Bay of Bengal. J Geophys Res Oceans 119: 3926–3947.

Akhil VP, Lengaigne M, Vialard J, Durand F, Keerthi MG, Chaitanya AVS, Papa F, Gopalakrishna VV, de Boyer Montegut C (2016) A modeling study of processes controlling the Bay of Bengal sea surface salinity interannual variability. J Geophys Res Oceans 121: 8471–8495.

Anil N, Ramesh Kumar MR, Sajeev R, Saji PK (2016) Role of distinct flavors of IOD events on Indian summer monsoon. Natural Hazards 82(2): 1317-1326.

Ashok K, Guan Z, Yamagata T (2001) Impact of the Indian Ocean Dipole on the relationship between the Indian monsoon rainfall and ENSO. Geophys Res Lett 28 (23): 4499-4502.

Ashok K, Guan ZY, Saji NH, Yamagata T (2004) Individual and combined influences of ENSO and the Indian Ocean Dipole on the Indian summer monsoon. J Clim 17: 3141-3155.

Behera SK, Ratnam JV (2018) Quasi-asymmetric response of the Indian summer monsoon rainfall to opposite phases of the IOD. Sci Rep 8:123. https://doi.org/10.1038/s41598-017-18396-6.

Bingham FM, Lee T (2017) Space and time scales of sea surface salinity and freshwater forcing variability in the global ocean (60S-60N). J Geophys Res Oceans 122:2909-2922.

Bonjean F, Lagerloef GSE (2002) Diagnostic model and analysis of the surface currents in the Tropical Pacific Ocean. J Phys Oceanogr 32 (10): 2938–2954.

Cabanes C, and Coauthors (2013) The CORA dataset: Validation and diagnostics of in-situ ocean temperature and salinity measurements. Ocean Sci 9: 1–18.

Chaitanya AVS, Lengaigne M, Vialard J, Gopalakrishna VV, Durand F, Krantikumar C, Suneel V, Papa F, Ravichandran M (2014) Fishermen-operated salinity measurements reveal a ‘‘river in the sea’’ flowing along the east coast of India. Bull Am Meterol Soc 95:1897–1908.

D'Addezio JM, Subrahmanyam B, Nyadjro ES, Murty VSN (2015) Seasonal variability of salinity and salt transports in the North Indian Ocean. J Phys Oceanogr 45(7): 1947-1966.

Dandapat S, Chakraborty A, Kuttippurath J (2018) Interannual variability and characteristics of the East India Coastal Current associated with Indian Ocean Dipole events using a high resolution regional ocean model. Ocean Dyn 68: 1321–1334.

de Boyer Montégut C, Madec G, Fischer AS, Lazar A, Iudicone D (2004) Mixed layer depth over the global ocean: An examination of profile data and a profile-based climatology. J Geophys Res 109, C12003. https://doi.org/10.1029/2004JC002378.

Delcroix T, Henin C (1991) Seasonal and Interannual variations of the sea surface salinity in the tropical Pacific Ocean. J Geophys Res 96: 22135–22150.

Du Y, Qu T, Meyers G, Masumoto Y, Sasaki H (2005) Seasonal heat budget in the mixed layer of the southeastern tropical Indian Ocean in a high-resolution ocean general circulation model. J Geophys Res 110, C04012, doi:10.1029/2004JC002845.

Du Y, Zhang Y, Zhang L.-Y, Tozuka T, Ng B, Cai W (2020) Thermocline warming induced extreme Indian Ocean dipole in 2019. Geophys Res Lett 47, e2020GL090079.

Ducet N, Le Traon P-Y, Reverdin F (2000) Global high-resolution mapping of ocean circulation from TOPEX/Poseidon and ERS-1/2. J Geophys Res 105: 19477–19498.

Foltz GR, McPhaden MJ (2008) Seasonal mixed layer salinity balance of the tropical North Atlantic Ocean. J Geophys Res Oceans 113, C02013, doi: 10.1029/2007JC004178.

Fournier S, Vialard J, Lengaigne M, Lee T, Gierach MM, Chaitanya AVS (2017) Modulation of the Ganges-Brahmaputra River plume by the Indian Ocean dipole and eddies inferred from satellite observations. J Geophys Res Oceans 122, 9591–9604.

Gadgil S, Joseph PV, Joshi NV (1984) Ocean atmosphere coupling over monsoon regions. Nature 312: 141–143.

Gnanaseelan C, Deshpande A, McPhaden MJ (2012) Impact of Indian Ocean Dipole and El Niño/Southern oscillation wind-forcing on the Wyrtki jets. J Geophys Res. 117, C08005, doi:10.1029/2012JC007918.

Greaser SR, Subrahmanyam B, Trott CB, Roman-Stork HL (2020) Interactions between mesoscale eddies and synoptic oscillations in the Bay of Bengal during the strong monsoon of 2019. J Geophys Res 125, e2020JC016772. https://doi.org/10.1029/2020JC016772.

Grodsky SA, Reul N, Bentamy A, Vandemark D, Guimbard S (2019) Eastern Mediterranean salinification observed in satellite salinity from SMAP mission. J Mar Sys 198: 103190, https://doi.org/10.1016/j.jmarsys.2019.103190.

Grunseich G, Subrahmanyam B, Murty VSN, Giese BS (2011) Sea surface salinity variability during the Indian Ocean Dipole and ENSO events in the tropical Indian Ocean. J Geophys Res 116, C11013, doi:10.1029/2011JC007456.

Han W, McCreary JP (2001) Modeling salinity distributions in the Indian Ocean. J Geophys Res 106: 859–877.

Horii T, Ueki I, Ando K (2018) Coastal upwelling events along the southern coast of Java during the 2008 positive Indian Ocean Dipole. J Oceanogr 74: 499–508.

Horii T, Ueki I, Ando K (2020) Coastal upwelling events, salinity stratification, and barrier layer observed along the southwestern coast of Sumatra. J Geophys Res Oceans, 125, e2020JC016287.

Hu S, Sprintall J (2016) Interannual variability of the Indonesian Throughflow: The salinity effect. J Geophys Res Oceans 121: 2596–2615.

Huffman GJ and Bolvin DT (2012) GPCP version 2.2 combined precipitation data set documentation, Lab. Atmos., NASA, Greenbelt, MD, USA. [Online]. Available: ftp://precip.gsfc.nasa.gov/pub/gpcp-v2.2/doc/V2.2_doc.pdf

Jensen TG (2001) Arabian Sea and Bay of Bengal exchange of salt and tracers in an ocean model. Geophys Res Lett 28: 3967–3970.

Jury MR (2019) Factors underlying changes in salinity around the southeastern Antilles. J Mar Syst 199:103208.

Kido S, Tozuka T (2017) Salinity variability associated with the positive Indian Ocean dipole and its impact on the upper ocean temperature. J Clim 30(19): 7885–7907.

Li Y, Wang F, Han W (2013) Interannual sea surface salinity variations observed in the tropical North Pacific Ocean. Geophys Res Lett 40(10): 2194–2199.

Lu B, Ren H.-L (2020) What caused the extreme Indian Ocean Dipole event in 2019? Geophys Res Lett 47, e2020GL087768. https://doi.org/10.1029/2020GL087768.

Masson S, Menkes C, Delecluse P, Boulanger J-P (2003) Impacts of salinity on the eastern Indian Ocean during the termination of the fall Wyrtki Jet. J Geophys Res Oceans, 108(C3), 3067, doi: 10.1029/2001JC000833.

McCreary JP, Han W, Shankar D, Shetye SR (1996) Dynamics of the East India coastal current. Numerical solutions. J Geophys Res 101(C6): 13993–14000.

McPhaden MJ, Nagura M (2014) Indian Ocean Dipole interpreted in terms of Recharge Oscillator theory. Clim Dyn 42: 1569–1586.

Mears CA, Scott J, Wentz FJ, Ricciardulli L, Leidner SM, Hoffman R, Atlas R (2019) A Near-Real-Time Version of the Cross-Calibrated Multiplatform (CCMP) Ocean Surface Wind Velocity Data Set. J Geophys Res Oceans 124: 6997–7010.

Menezes VV (2020) Statistical Assessment of Sea-Surface Salinity from SMAP: Arabian Sea, Bay of Bengal, and a Promising Red Sea Application. Remote Sens 12, 447; doi:10.3390/rs12030447.

Murtugudde R, McCreary Jr. JP, Busalacchi AJ (2000) Oceanic processes associated with anomalous events in the Indian Ocean with relevance to 1997–1998. J Geophys Res 105: 3295–3306.

Murty VSN, Sarma YYB, Rao DP, Murty CS (1992) Water characteristics, mixing and circulation in the Bay of Bengal during southwest monsoon. J Mar Res 50: 207–228.

Murty VSN, Sarma YYB, Rao DP (1996) Variability of the oceanic boundary layer characteristics in the northern Bay of Bengal during MONTBLEX-90. Earth Planet Sci Lett 105: 41–61.

Nichols RE, Subrahmanyam B (2019) Estimation of Surface Freshwater Fluxes in the Arctic Ocean Using Satellite-Derived Salinity. Remote Sens Earth Syst Sci 2: 247–259.

Nyadjro ES, McPhaden MJ (2014) Variability of zonal currents in the equatorial Indian Ocean on seasonal to interannual time scales. J Geophys Res 119, doi: 10.1002/2014JC010380.

Nyadjro ES, Rydbeck AV, Jensen TG, Richman JG, Shriver JF (2020) On the Generation and Salinity Impacts of Intraseasonal Westward Jets in the Equatorial Indian Ocean. J Geophys Res 125, https://doi.org/10.1029/2020JC016066.

Nyadjro ES, Subrahmanyam B (2014) SMOS satellite mission reveals the salinity structure of the Indian Ocean Dipole. IEEE Geosci Remote Sens Lett 11 (9): 1564-1568.

Nyadjro ES, Subrahmanyam B, Murty VSN, Shriver JF (2010) Salt transport in the near-surface layer in the monsoon-influenced Indian Ocean using HYCOM. Geophys Res Lett 37, L15603, doi:10.1029/2010GL044127.

Nyadjro ES, Subrahmanyam B, Murty VSN, Shriver JF (2012) The role of salinity on the dynamics of the Arabian Sea mini warm pool. J Geophys Res 117, C09002, doi:10.1029/2012JC007978.

Pant V, Girishkumar MS, Udaya Bhaskar TVS, Ravichandran M, Papa F, Thangaprakash VP (2015) Observed interannual variability of near-surface salinity in the Bay of Bengal. J Geophys Res Oceans 120: 3315–3329.

Qi J, Zhang L, Qu T, Yin B, Xu Z, Yang D, Li D, Qin Y (2019) Salinity variability in the tropical Pacific during the Central-Pacific and Eastern-Pacific El Niño events. J Mar Syst 199, 103225.

Rao RR, Girish Kumar MS, Ravichandran M, Rao AR, Gopalakrishna VV, Thadathil P (2010) Interannual variability of Kelvin wave propagation in the wave guides of the equatorial Indian Ocean, the coastal Bay of Bengal, and the southeastern Arabian Sea during 1993–2006. Deep-Sea Res I 57:1–13.

Rao RR, Sivakumar R (2003) Seasonal variability of sea surface salinity and salt budget of the mixed layer of the north Indian Ocean. J Geophys Res 108(C1), 3009, doi:10.1029/2001JC000907.

Ratna SB, Cherchi A, Osborn TJ, Joshi M, Uppara U (2021) The extreme positive Indian Ocean dipole of 2019 and associated Indian summer monsoon rainfall response. Geophys Res Lett 48, e2020GL091497. https://doi.org/10.1029/2020GL091497.

Reynolds RW, Smith TM, Liu C, Chelton DB, Casey KS, Schlax MG (2007) Daily High-Resolution-Blended Analyses for Sea Surface Temperature. J Clim 20: 5473-5496.

Roman-Stork HL, Subrahmanyam B, Murty VSN (2020) The role of salinity in the southeastern Arabian Sea in determining monsoon onset and strength. J Geophys Res Oceans 125, e2019JC015592.

Saji NH, Yamagata T (2003) Structure of SST and surface wind variability during Indian Ocean Dipole Mode events: COADS observations. J Clim 16: 2735–2751.

Schott F, McCreary JP (2001) The monsoon circulation of the Indian Ocean. Prog Oceanogr 51: 1–123.

Sengupta D, Bharath Raj GN, Shenoi SSC (2006) Surface freshwater from Bay of Bengal runoff and Indonesian Throughflow in the tropical Indian Ocean. Geophys Res Lett 33, L22609, doi:10.1029/2006GL027573.

Shankar D, McCreary JP, Han W, Shetye SR (1996) Dynamics of the East India coastal current. 1. Analytic solutions forced by interior Ekman pumping and local alongshore winds. J Geophys Res 101(C6):13975–13991.

Subrahmanyam B, Roman-Stork HL, Murty VSN (2020) Response of the Bay of Bengal to 3-7-day synoptic oscillations during the southwest monsoon of 2019. J Geophys Res 125, e2020JC016200. https://doi.org/ 10.1029/2020JC016200.

Subrahmanyam B, Trott CB, Murty VSN (2018) Detection of intraseasonal oscillations in SMAP salinity in the Bay of Bengal. Geophys Res Lett 45: 7057-7065.

Susanto RD, Gordon AL, Zheng Q (2001) Upwelling along the coast of Java and Sumatra and its relation to ENSO. Geophys Res Lett 28: 1599–1602.

Thompson B, Gnanaseelan C, Salvekar PS (2006) Variability in the Indian Ocean circulation and salinity and its impact on SST anomalies during dipole events. J Mar Res 64(6): 853–880.

Trott CB, Subrahmanyam B, Murty VSN, Shriver JF (2019) Large scale fresh and saltwater exchanges in the Indian Ocean. J Geophys Res, https://doi.org/10.1029/2019JC015361.67.

Wang G, Cai W, Yang K, Santoso A, Yamagata T (2020) A unique feature of the 2019 extreme positive Indian Ocean Dipole event. Geophys Res Lett 47, e2020GL088615. https://doi.org/10.1029/2020GL088615.

Webster PJ, Moore AM, Loschnigg JP, Leben RR (1999) Coupled ocean–atmosphere dynamics in the Indian Ocean during 1997–98. Nature 401: 356–360.

Zhang L, Du Y, Cai W (2018) Low-frequency variability and the unusual Indian Ocean Dipole events in 2015 and 2016. Geophys Res Lett 45: 1040–1048.

Zhang Y, Du Y, Zheng S, Yang Y, Cheng X (2013) Impact of Indian Ocean Dipole on the salinity budget in the equatorial Indian Ocean. J Geophys Res Oceans 118: 4911–4923.

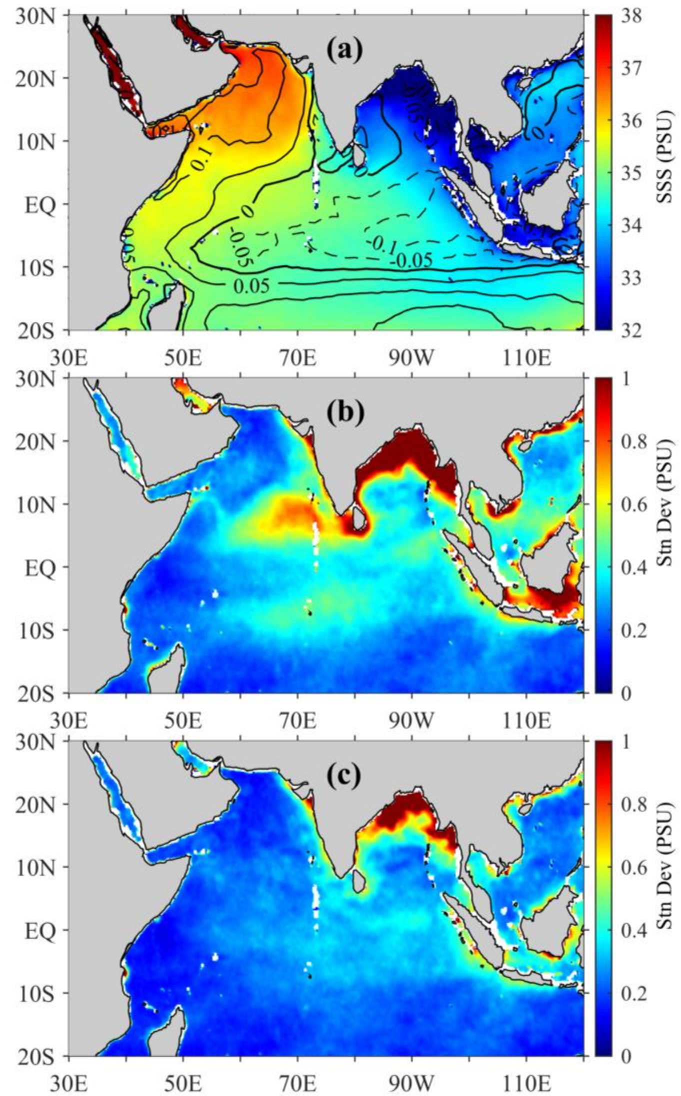

Fig. 1. (a) Annual mean (computed for April 2015-December 2020) SSS (color shading, PSU), and evaporation minus precipitation (E-P, contours, m month^{-1}). Solid contours show evaporation exceeds precipitation while dashed contours show precipitation exceeds evaporation. CI= 0.05 m month^{-1}. Standard deviation of (b) seasonal SSS anomalies (PSU), and (c) interannual SSS anomalies (PSU).

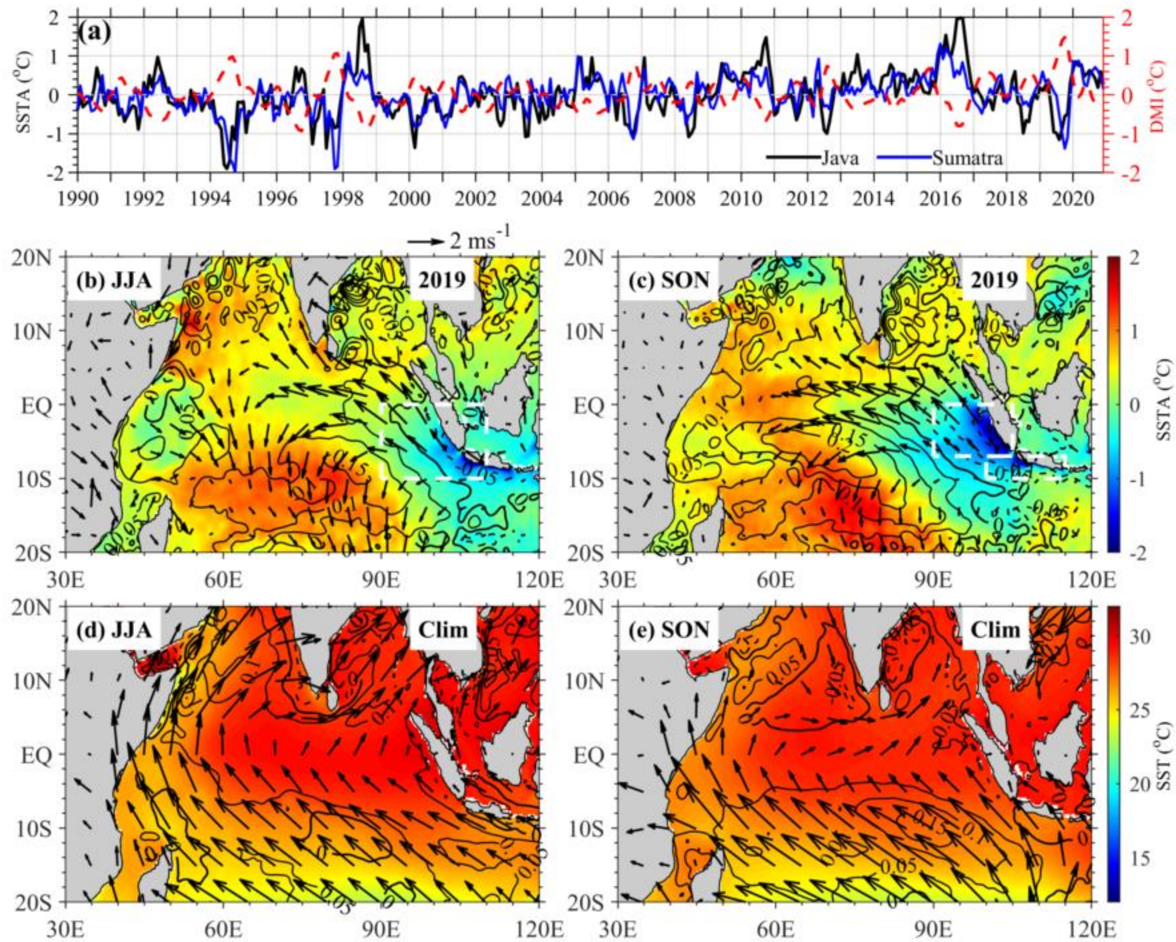

Fig. 2. (a) Dipole mode index (DMI, red line, °C), sea surface temperature interannual anomalies (SSTA, °C) box-averaged over Java (100°E-115°E, 7°S-10°S; black line) and Sumatra (90°E-105°E, 7°S-EQ; blue line) during 1990-2020. Composite mean of interannual anomalies of SST (color shading, °C), surface winds (vectors, ms^{-1}), and SSH (contours, m) during (b) June-August 2019 and (c) September-November 2019. Composite mean of climatological sea surface temperature (SST, color shading, °C), surface winds (vectors, ms^{-1}), and sea surface height (SSH, contours, m) during (d) June-August and (e) September-November. Solid contours show positive SSH while dashed contours show negative SSH. Box in (b) marks the SETIO region, 90°E-110°E, 10°S-0°S.

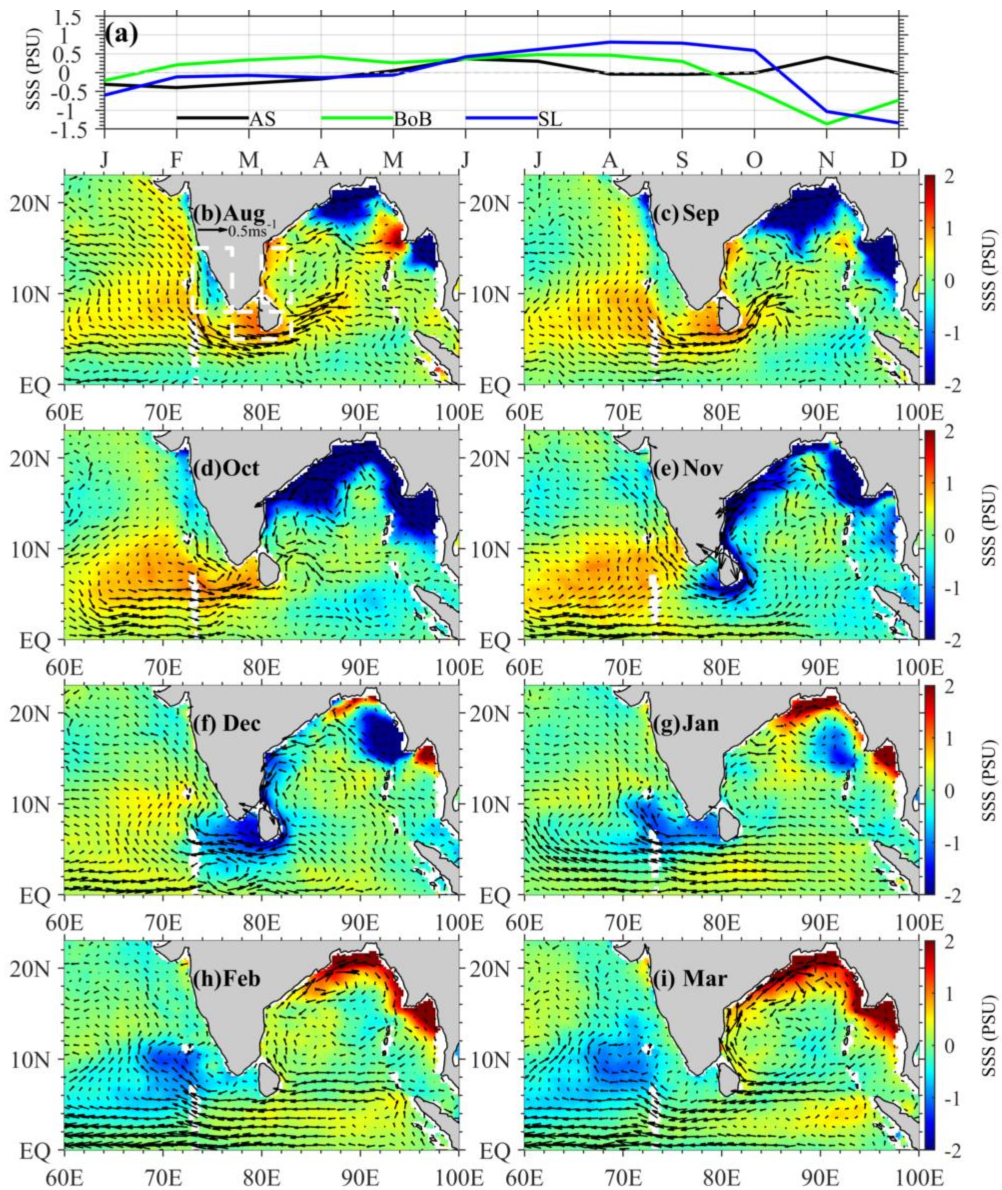

Fig. 3. (a) Climatological seasonal anomalies of sea surface salinity (SSS, PSU) box-averaged over the Arabian Sea (black line), Bay of Bengal (green line), and Sri Lanka (blue line). Climatological seasonal anomalies of SSS (color shading, PSU), and OSCAR surface currents (vectors, ms^{-1}) in the northern Indian Ocean during (b) August, (c) September, (d) October, (e) November, (f) December, (g) January, (h) February, and (i) March. The climatological seasonal anomalies are computed as the difference between monthly climatologies and the data mean, where means are computed over the period covering the SMAP data for this study (i.e., April 2015-December 2020).

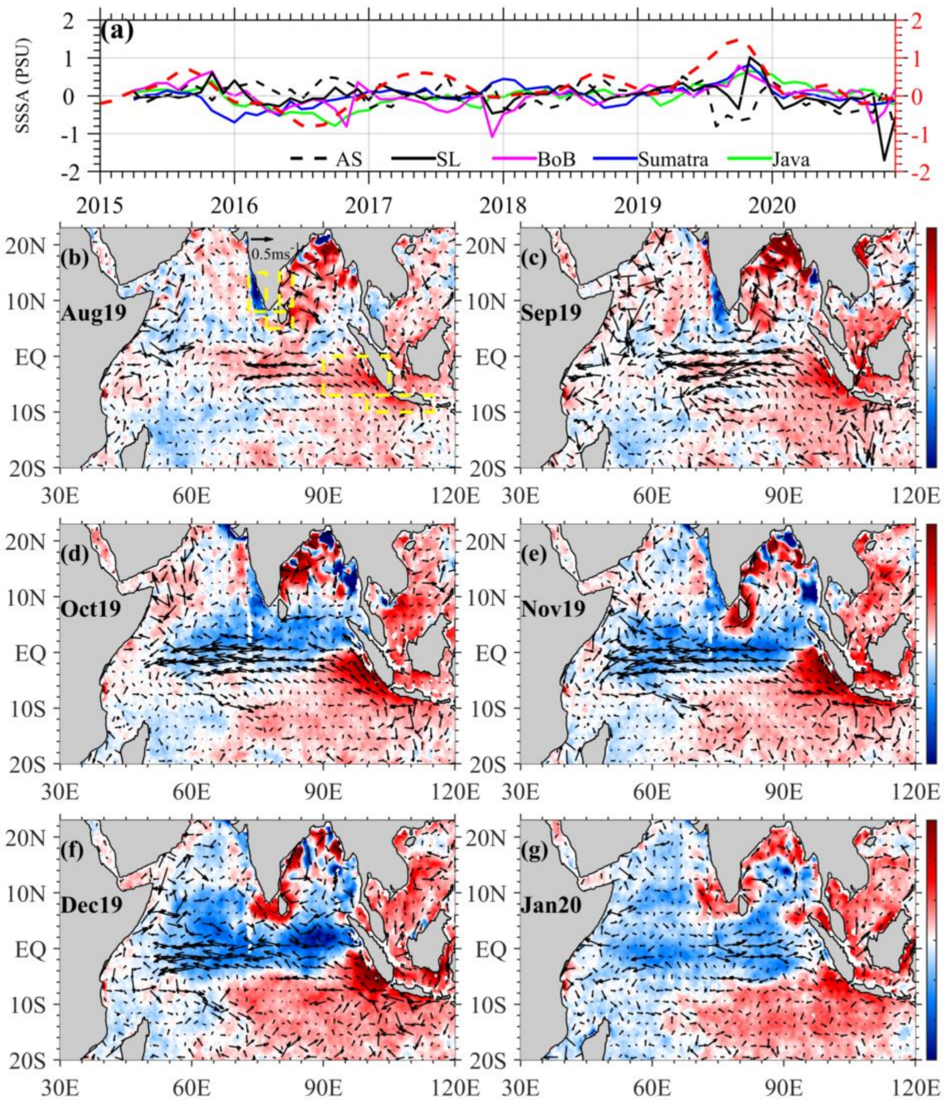

Fig. 4. (a) Dipole mode index (DMI, red line, °C), sea surface salinity interannual anomalies (SSSA, PSU) box-averaged over the Arabian Sea (dashed black line), Sri Lanka (solid black line), Bay of Bengal (solid magenta line), Sumatra (solid blue line), and Java (solid green line). SSSA (color shading, PSU), and surface currents interannual anomalies (vectors, ms^{-1}) during (b) August 2019, (c) September 2019, (d) October 2019, (e) November 2019, (f) December 2019, and (g) January 2020.

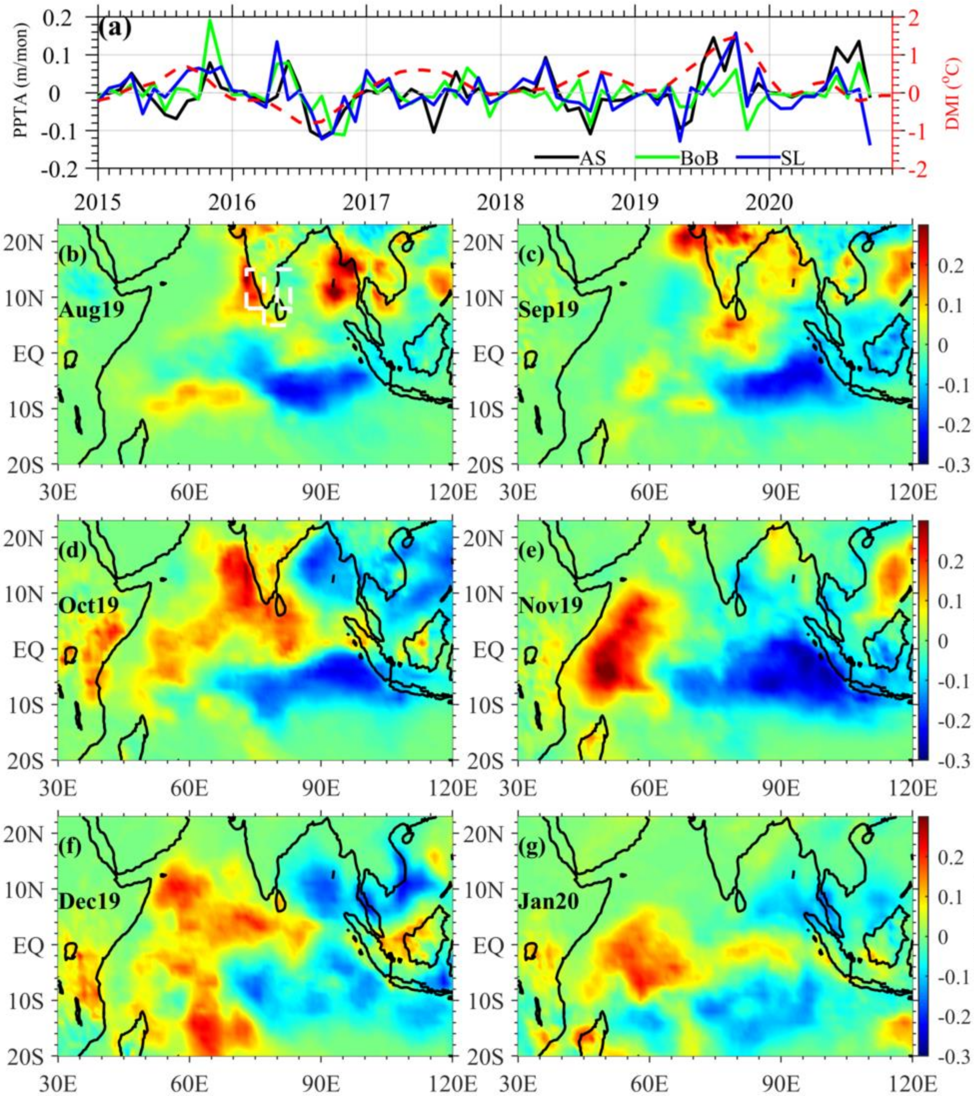

Fig. 5. (a) Dipole mode index (DMI, red line, °C), precipitation interannual anomalies (PPTA, m month^{-1}) box-averaged over the Arabian Sea (black line), Bay of Bengal (green line), and Sri Lanka (blue line). PPTA (color shading, m month^{-1}) during (b) August 2019, (c) September 2019, (d) October 2019, (e) November 2019, (f) December 2019, and (g) January 2020.

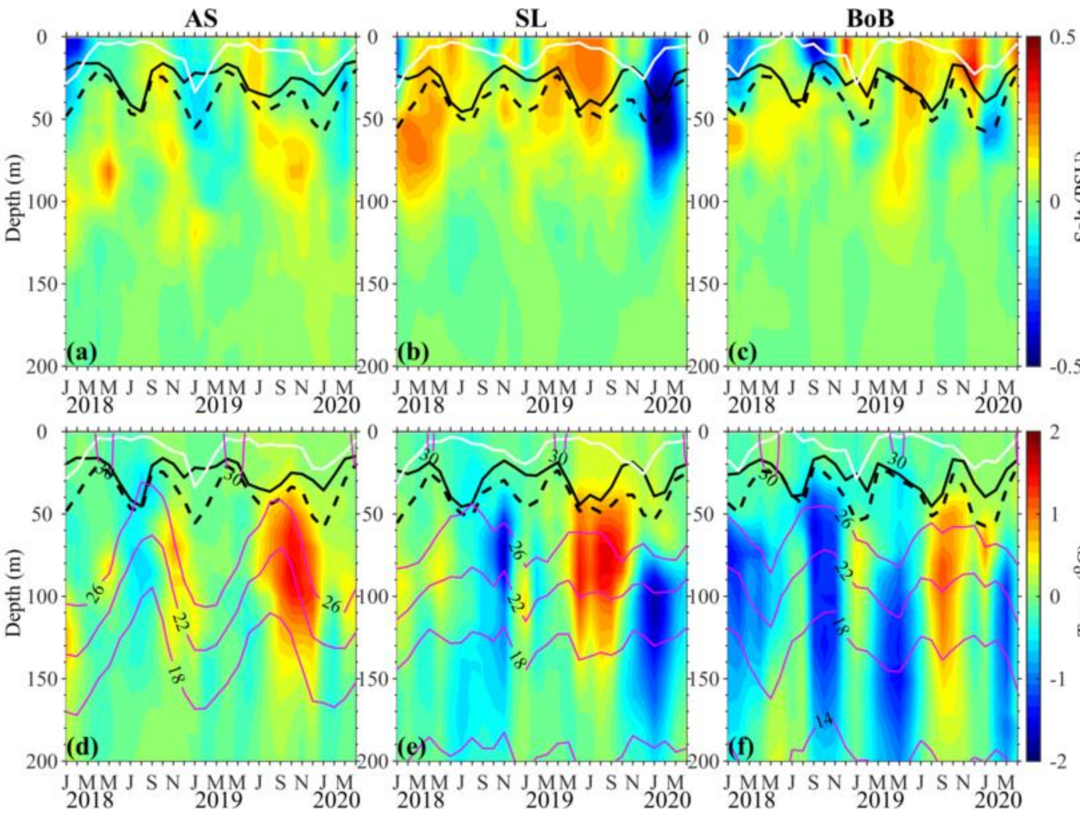

Fig. 6. Time-depth sections of CORA interannual anomalies of (top row) salinity (color shading, PSU), and (bottom row) temperature (color shading, °C), box-averaged over (left column) Arabian Sea, (middle column) Sri Lanka, and (right column) Bay of Bengal. Solid magenta lines show isotherms (°C, CI=4°C), solid black lines show the mixed layer depth (MLD, m), dashed black lines show the isothermal layer depth (ILD, m), and the solid white lines show the barrier layer thickness (BLT = ILD-MLD). See Fig. 4b for locations of boxes.

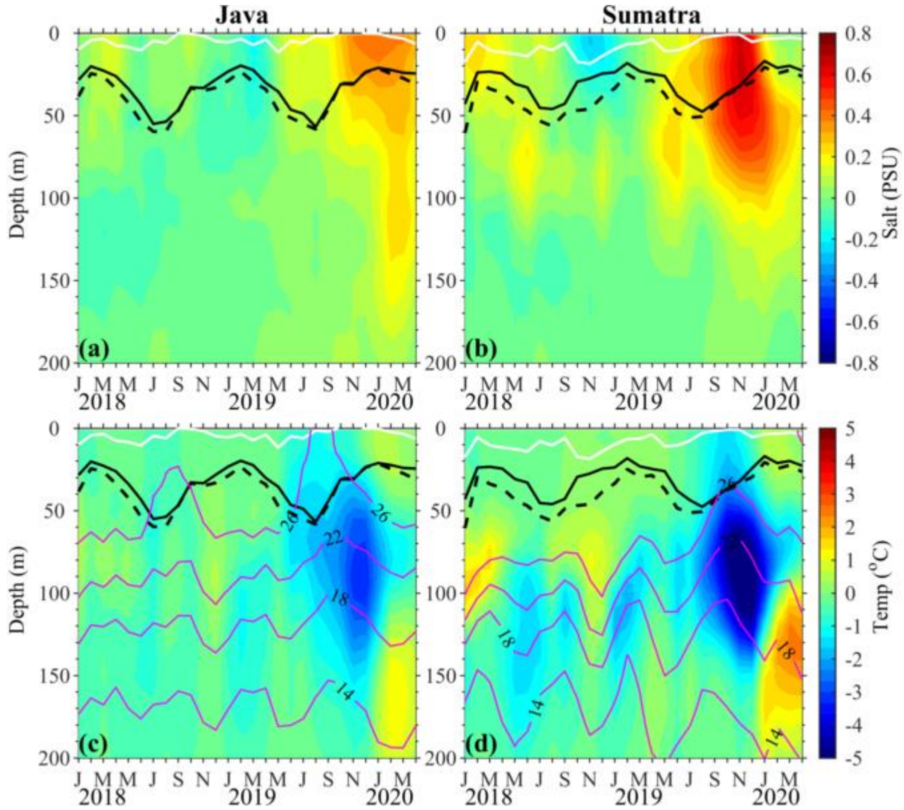

Fig. 7. Time-depth sections of CORA interannual anomalies of (top row) salinity (color shading, PSU), and (bottom row) temperature (color shading, °C), box-averaged over (left column) Java, and (right column) Sumatra. Solid magenta lines show isotherms (°C, CI=4°C), solid black lines show the mixed layer depth (MLD, m), dashed black lines show the isothermal layer depth (ILD, m), and the solid white lines show the barrier layer thickness (BLT = ILD-MLD). See Fig. 4b for locations of boxes.

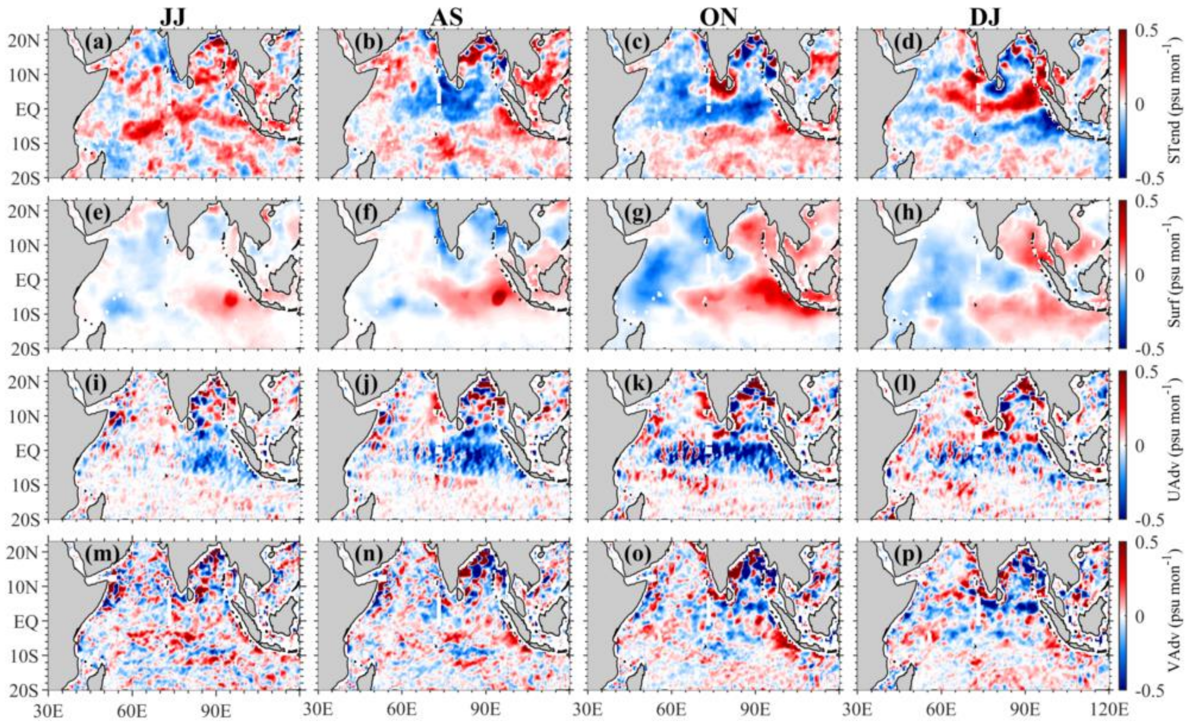

Fig. 8. Bi-monthly composites of interannual salt budget terms (psu month^{-1}) for (row 1) salinity tendency, (row 2) surface freshwater flux, (row 3) zonal advection (UADV), and (row 4) meridional advection (VADV), during (column 1) June-July 2019, (column 2) August-September 2019, (column 3) October-November 2019, and (column 4) December 2019-January 2020. See equation (2) for definition of salt budget terms.